九州大学学術情報リポジトリ
Kyushu University Institutional Repository

Cholesterol sulfate is a DOCK2 inhibitor that mediates tissue-specific immune evasion in the eye

櫻井, 哲哉

https://hdl.handle.net/2324/4060039

出版情報：Kyushu University, 2019, 博士（医学）, 課程博士
バージョン：
権利関係：© The Authors

KYUSHU UNIVERSITY

INFLAMMATION

Cholesterol sulfate is a DOCK2 inhibitor that mediates tissue-specific immune evasion in the eye

Tetsuya Sakurai[1]*, Takehito Uruno[1,2]*, Yuki Sugiura[3,4], Takaaki Tatsuguchi[1], Kazuhiko Yamamura[1†], Miho Ushijima[1‡], Yuko Hattori[3], Mutsuko Kukimoto-Niino[5], Chiemi Mishima-Tsumagari[5], Mayuki Watanabe[1§], Makoto Suematsu[3], Yoshinori Fukui[1,2||]

Copyright © 2018 The Authors, some rights reserved; exclusive licensee American Association for the Advancement of Science. No claim to original U.S. Government Works

Although immune responses are essential to protect the body from infection, they can also harm tissues. Certain tissues and organs, including the eye, constitute specialized microenvironments that locally inhibit immune reactivity. Dedicator of cytokinesis protein 2 (DOCK2) is a Rac-specific guanine nucleotide exchange factor (GEF) that is predominantly found in hematopoietic cells. DOCK2 plays a key role in immune surveillance because it is essential for the activation and migration of leukocytes. *DOCK2* mutations cause severe immunodeficiency in humans. We found that DOCK2-mediated Rac activation and leukocyte migration were effectively inhibited by cholesterol sulfate (CS), but not by cholesterol or other sulfated steroids. CS bound to the catalytic domain of DOCK2 and suppressed its GEF activity. Mass spectrometric quantification revealed that CS was most abundantly produced in the Harderian gland, which provides the lipids that form the oily layer of the tear film. Sulfation of cholesterol is mediated by the sulfotransferases SULT2B1b and, to a lesser extent, SULT2B1a, which are produced from the same gene through alternative splicing. By genetically inactivating *Sult2b1*, we showed that the lack of CS in mice augmented ultraviolet- and antigen-induced ocular surface inflammation, which was suppressed by administration of eye drops containing CS. Thus, CS is a naturally occurring DOCK2 inhibitor and contributes to the generation of the immunosuppressive microenvironment in the eye.

INTRODUCTION

The immune system has evolved to recognize and interact with microorganisms to protect the body from infection. Leukocytes continually patrol the body to identify invading pathogens and elicit immune responses against them. However, immune responses generally carry a risk for damaging or impairing the function of vital tissues and therefore could threaten the survival of the host (*1*, *2*). Certain tissues and organs, such as the brain and the pregnant uterus, constitute specialized microenvironments that locally inhibit immune reactivity (*3*–*5*). Although this phenomenon is classically known as immune privilege, various other tissues also create microenvironments that help them evade the immune system. Among these are tumors (*6*), in which local immunosuppressive mechanisms predominate over stimulatory immune responses. Several molecular and cellular mechanisms that suppress tissue inflammation have been reported. These include the production of cell-surface molecules, such as the Fas ligand or programmed cell death ligand 1, secretion of the anti-inflammatory cytokine interleukin-10 or transforming growth factor–β, and induction of intracellular enzymes with immunoregulatory effects, such as indoleamine 2,3-dioxygenase, arginase, or inducible nitric oxide synthase (*7*–*10*). Although it seems reasonable to expect that bioactive lipids could contribute to immune evasion, no evidence for their participation in immune evasion has been reported.

Dedicator of cytokinesis protein 2 (DOCK2) is a member of the CDM family of proteins, named for *Caenorhabditis elegans* cell-death abnormal (CED)–5, mammalian DOCK1 and DOCK5, and *Drosophila melanogaster* Myoblast City, and is predominantly found in hematopoietic cells (*11*). Although DOCK2 does not contain Dbl homology (DH) and pleckstrin homology (PH) domains, which are typically found in guanine nucleotide exchange factors (GEFs), DOCK2 mediates the exchange of guanosine diphosphate (GDP) for guanosine triphosphate (GTP) on the guanosine triphosphatase Rac through its DOCK homology region–2 (DHR-2) domain (*12*, *13*). DOCK2 is a major Rac GEF acting downstream of chemoattractant receptors and antigen receptors in lymphocytes, neutrophils, and natural killer cells and plays key roles in the migration and activation of these cell types (*14*–*17*). Consistent with this, deletion of *Dock2* in mice prevents cardiac allograft rejection and the development of autoimmune disease (*18*, *19*). *DOCK2* mutations also cause severe immunodeficiency in humans (*20*). Thus, DOCK2 is essential for immune surveillance and immune responses in both humans and mice.

Sulfonation plays an important role in the biological activity of many endogenous molecules. Cholesterol sulfate (CS) is a sulfated derivative of cholesterol and is widely distributed in various tissues and body fluids (*21*). In skin, CS is located predominantly in the epidermis, where it contributes to epidermal differentiation as well as to the development and maintenance of the epidermal barrier function (*21*–*25*). In addition, CS has been implicated in many biological processes including sperm capacitation, platelet adhesion, blood clotting, leukotriene biosynthesis, and T cell receptor signaling (*26*–*30*). However, its physiological functions and the underlying mechanisms are not fully understood. Here, we identified CS as a naturally occurring DOCK2 inhibitor. Under physiological conditions, CS was

[1]Division of Immunogenetics, Department of Immunobiology and Neuroscience, Medical Institute of Bioregulation, Kyushu University, Fukuoka 812-8582, Japan. [2]Research Center for Advanced Immunology, Kyushu University, Fukuoka 812-8582, Japan. [3]Department of Biochemistry, Keio University School of Medicine, Tokyo 160-8582, Japan. [4]Precursory Research for Embryonic Science and Technology, Japan Science and Technology Agency, Tokyo 102-0075, Japan. [5]RIKEN Center for Life Science Technologies, Yokohama 230-0045, Japan.
*These authors contributed equally to this work.
†Present address: Department of Dermatology, Graduate School of Medical Sciences, Kyushu University, Fukuoka 812-8582, Japan.
‡Present address: Department of Urology, Graduate School of Medical Sciences, Kyushu University, Fukuoka 812-8582, Japan.
§Present address: Japan Agency for Medical Research and Development, Tokyo 100-0004, Japan.
||Corresponding author. Email: fukui@bioreg.kyushu-u.ac.jp

Downloaded from http://stke.sciencemag.org/ on August 12, 2018

most abundantly produced in mice in the Harderian gland, which provides lipids to form the oily layer of the tear film (*31*). Although the lack of CS augmented ultraviolet (UV)– and antigen-induced ocular surface inflammation, administration of eye drops containing CS limited this inflammatory response. Our results thus indicate that CS mediates immune evasion in the eye by inhibiting DOCK2.

RESULTS

CS binds to the DHR-2 domain of DOCK2 and inhibits its GEF activity

Because DOCK2 deficiency suppresses allograft rejection and autoimmune disease development in mice (*18*, *19*), DOCK2 could serve as a molecular target controlling inflammatory responses. To search for potential DOCK2 inhibitors, we screened 577 pharmacologically active compounds for their ability to inhibit DOCK2-mediated Rac activation in vitro and identified CS (Fig. 1A) as a candidate. CS inhibited the Rac GEF activity of the DHR-2 domain of murine DOCK2 in vitro in a dose-dependent manner with a half-maximal inhibitory concentration (IC_{50}) of 2.0 μM (Fig. 1, B and C). Similar results were obtained using the DHR-2 domain of human (fig. S1A). Although CS also inhibited murine DOCK1 and DOCK5 (fig. S1B), CS did not affect Rac activation mediated by the other DH-type GEFs Tiam1 and Trio at any of the tested concentrations (Fig. 1B and fig. S1C). When the sulfate moiety of CS was removed or replaced with acetate, the resulting compounds, cholesterol, or cholesterol acetate (CA), respectively, exhibited greatly reduced DOCK2 inhibitory activity (Fig. 1C). Similarly, other sulfated steroids such as pregnenolone sulfate (PREGS), dehydroepiandrosterone sulfate (DHEAS), estrone sulfate (E1S), estradiol sulfate (E2S), and estriol sulfate (E3S) failed to inhibit the Rac GEF activity of DOCK2 (Fig. 1C). These results indicate that both the sulfate moiety and the cholesterol side chain are required for the inhibitory activity of CS. Surface plasmon resonance (SPR)–based binding assays revealed that CS directly bound to the DOCK2 DHR-2 domain with a dissociation constant of 9.9 μM (Fig. 1D). This binding was specific because cholesterol derivatives other than CS did not show any binding to DOCK2 DHR-2 (Fig. 1E). Consistent with this finding, the association between DOCK2 DHR-2 and Rac1 was abrogated in the presence of CS, but not in the presence of cholesterol or CA (Fig. 1F). Thus, CS is a naturally occurring DOCK2 inhibitor that binds to the DHR-2 domain and blocks DOCK2 Rac GEF activity.

CS inhibits DOCK2-mediated Rac activation and cellular functions

Migration of lymphocytes and neutrophils in mice and humans critically depends on DOCK2 (*14*, *16*, *20*). To examine whether CS inhibits DOCK2 activity in cells, we first analyzed the effect of CS on lymphocyte migration. In Transwell chemotaxis assays, CS effectively inhibited the migratory response of murine T cells to the chemokine CCL21 in a concentration-dependent manner, similar to the knockout of *Dock2* (Fig. 2A). In addition, murine bone marrow (BM)–derived neutrophils treated with CS exhibited a migration defect toward the chemoattractant *N*-formyl-Met-Leu-Phe (*f*MLP) (Fig. 2B). Similar results were obtained when human peripheral blood T cells and neutrophils were analyzed in the same chemotaxis assays (fig. S2, A and B). This inhibitory effect was specific to CS because other cholesterol derivatives did not affect migration of murine lymphocytes (Fig. 2C). Consistent with these functional defects in chemotaxis, CS treatment markedly suppressed CCL21- and *f*MLP-induced Rac activation in murine T cells and neutrophils, respectively (Fig. 2D). We also found that neutrophils undergoing chemotaxis stopped migration at a defined distance when CS was added to the *f*MLP source (Fig. 2E and movie S1). However, such an effect was not observed by adding DHEAS to the *f*MLP source (Fig. 2E and movie S1). These results indicate that CS blocks leukocyte migration, likely by inhibiting the DOCK2-mediated Rac activation.

CS is most abundantly produced in the Harderian gland

Sulfation is catalyzed by members of the sulfotransferase (SULT) family of sulfate-conjugating enzymes (*32*). In both humans and mice, the SULT2B1a and SULT2B1b proteins are encoded by the same gene but differ in their N-terminal amino acid sequences as a result of alternative splicing (*21*, *33*–*35*). Whereas human SULT2B1a and SULT2B1b have unique 8– and 23–amino acid sequences N-terminal to the conserved region, murine SULT2B1a and SULT2B1b have additional 54– and 20–amino acid sequences at the N terminus, respectively (Fig. 3A) (*35*). A study using human recombinant proteins indicated that SULT2B1b, but not SULT2B1a, plays a major role in cholesterol sulfation (*36*). Similarly, we found that the in vitro cholesterol sulfation activity of recombinant murine SULT2B1b was seven times higher than that of murine SULT2B1a, with the two enzymes exhibiting V_{max} values of 11.2 and 1.6 nmol min^{-1} mg^{-1} and Michaelis constant (K_m) values of 2.6 and 1.0 μM, respectively (Fig. 3B). The recombinant enzymes used in these assays were expressed and purified as GST fusions, and the GST tag was removed before the cholesterol sulfation assays. We obtained similar kinetic data using a murine SULT2B1b that was expressed as a His-SUMO–tagged fusion protein and analyzed after removing the His-SUMO moiety with SUMO protease 1 (fig. S3; V_{max} of 12.3 nmol min^{-1} mg^{-1} and K_m value of 2.2 μM), although the extra peptide remaining on the N terminus of the two differently expressed recombinant proteins differed (see Materials and Methods). In addition, in both assays, none of our SULT2B1b recombinant proteins showed substrate inhibition (*37*) below 15 μM cholesterol (Fig. 3B and fig. S3).

To determine which tissues produce SULT2B1b, we developed a specific antibody that can distinguish SULT2B1b from SULT2B1a in mice (fig. S4, A to C). Western blot analyses revealed that SULT2B1b was present in the small intestine and skin in C57BL/6 (designated *Sult2b1*$^{+/+}$) mice (Fig. 3C), consistent with that previously reported for *Sult2b1b* mRNA expression (*34*). However, the highest abundance of SULT2B1b was detected in the Harderian gland (Fig. 3C), an orbital gland that produces the lipids that form the oily layer of the tear film (*31*). This was confirmed by a different antibody that was raised against the C-terminal sequence that is conserved between murine SULT2B1a and SULT2B1b and thus recognizes both isoforms (fig. S5, A to D). SULT2B1a was not detected in any tissues tested (fig. S5D). Endogenous cholesterol sulfating activity was much higher in the Harderian gland than in the small intestine or skin, the other tissues in which we detected SULT2B1b (Fig. 3D), and its activity correlated with the amount of SULT2B1b in each tissue (Fig. 3, C and D).

To understand the physiological function of SULT2B1b in more detail, we used knockout (KO) (*Sult2b1*$^{-/-}$) mice that had been generated by deleting exons 3 to 7 of the *Sult2b1* gene (fig. S6, A to C) (*30*, *38*). Although the Harderian gland of *Sult2b1*$^{+/+}$ mice contained more than 500 pmol of CS per milligram of tissue, the presence of CS and cholesterol sulfation activity were hardly detected in the Harderian gland of *Sult2b1*$^{-/-}$ mice (Fig. 3, E to G), indicating that CS production

Downloaded from http://stke.sciencemag.org/ on August 12, 2018

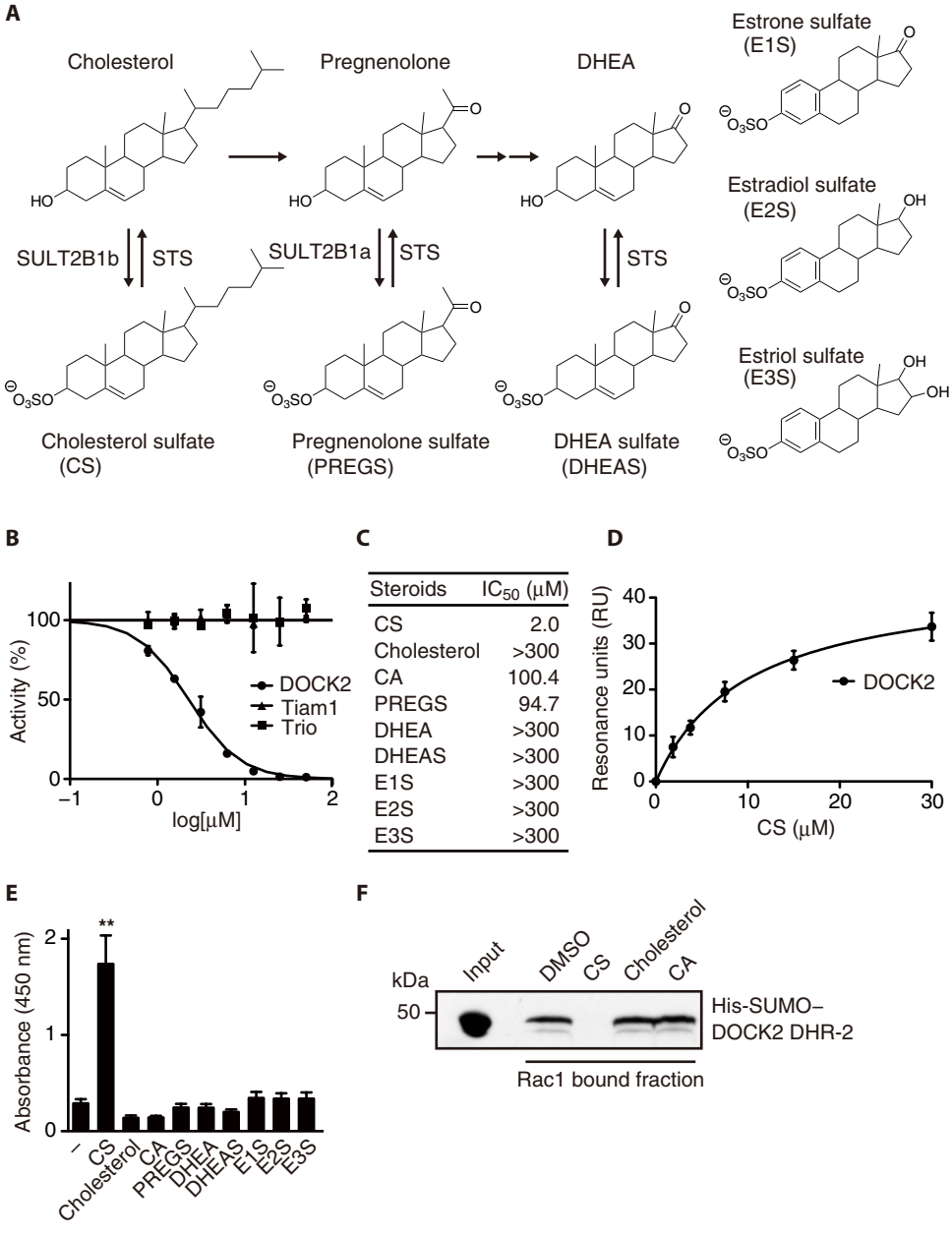

Fig. 1. CS inhibits the Rac GEF activity of the DHR2 domain of DOCK2. (**A**) Schematic representation of the sulfation and deconjugation pathways for cholesterol, pregnenolone, and DHEA and structures of estrogen sulfates. STS, steroid sulfatase. (**B**) In vitro Rac GEF activity of the DHR-2 domain of murine DOCK2 and the DH and PH domains of Tiam1 and Trio in the presence of the indicated concentrations of CS. Data were normalized to the activity of each GEF in the presence of vehicle alone (dimethyl sulfoxide (DMSO)]. Data are presented as means ± SD. $n = 3$ independent experiments. (**C**) IC_{50} values of CS and its analogs for the Rac GEF activity of murine DOCK2 DHR-2. Data represent means from three to five experiments. (**D**) Titration curve for CS binding to murine DOCK2 DHR-2. The resonance units (RUs) obtained from SPR-based binding assays were plotted as a function of the concentration of CS. Data are presented as means ± SD. $n = 9$ experiments. (**E**) Binding of murine DOCK2 DHR-2 to the indicated immobilized steroids. Data are presented as means ± SD. $n = 5$ experiments. $^{**}P < 0.01$ compared with uncoated (–) substrate [one-way analysis of variance (ANOVA) followed by Bonferroni post hoc test]. (**F**) Western blot showing His-SUMO–tagged murine DOCK2 DHR-2 pulled down with glutathione *S*-transferase (GST)–tagged Rac1 in vitro in the presence of CS, cholesterol, CA, or vehicle alone (DMSO). Input, in vitro reaction without pull down. Data are representative of three independent experiments.

critically depends on SULT2B1b in vivo. We also found that in mice heterozygous for the mutant allele (*Sult2b1*$^{+/-}$), the CS content in the Harderian gland was reduced to 58% of that of wild-type controls (Fig. 3E). Because this reduction was well correlated with the amount of SULT2B1b and its enzymatic activity in the Harderian gland (Fig. 3, F and G), gene dosage is likely to affect SULT2B1b-mediated cholesterol sulfation. By comparing the CS content in various tissues between *Sult2b1*$^{+/-}$ and *Sult2b1*$^{-/-}$ littermates, we confirmed that CS was most abundantly produced in the Harderian gland, as expected (Fig. 3H). In *Sult2b1*$^{+/-}$ mice, CS was also detected in tears at a concentration of 231.8 nM (Fig. 3I). Mass spectrometry imaging of the eye revealed that CS was present in the anterior chamber in the eye and the Harderian gland of *Sult2b1*$^{+/-}$ mice (Fig. 3J and fig. S7). In contrast, *Sult2b1*$^{-/-}$ mice had very low or undetectable amounts of CS in all tissues tested (Fig. 3, H to J, and fig. S7).

CS limits ocular surface inflammation

Acute UV exposure causes photokeratitis, which is initiated by apoptosis of corneal epithelial cells and is followed by recruitment of leukocytes into the anterior chamber, the aqueous humor–filled space between the cornea and iris, where they come into contact with and damage the corneal endothelium (*39*–*41*). To examine whether lack of CS aggravates the severity of photokeratitis, *Sult2b1*$^{+/-}$, and *Sult2b1*$^{-/-}$ mice were UV-irradiated under anesthesia. The thickness of the corneal epithelial layer was comparably reduced in both groups of mice 24 hours after UV irradiation (Fig. 4A), indicating that the presence or absence of CS did not affect the susceptibility of corneal cells to UV-induced apoptosis. However, inflammatory infiltrates in the anterior chamber were increased in *Sult2b1*$^{-/-}$ mice compared to in *Sult2b1*$^{+/-}$ mice (Fig. 4B). The majority of the inflammatory cells infiltrating the anterior chamber in both genotypes were Gr1^{+} neutrophils (fig. S8). Similarly, *Sult2b1* deficiency significantly augmented the infiltration of T cells into the conjunctiva in an experimental allergic conjunctivitis (EAC) model (Fig. 4, C and D), in which mice were sensitized and topically challenged with short ragweed (SRW) pollen (*42*).

SULT2B1b sulfates not only cholesterol but also oxysterols such as 25-hydroxycholesterol (25HC) (*35*, *43*–*45*). Although this sulfated product, 25-hydroxycholesterol-3-sulfate (25HCS) (fig. S9A), is known to induce anti-inflammatory responses (*46*), 25HCS did not affect

Downloaded from http://stke.sciencemag.org/ on August 12, 2018

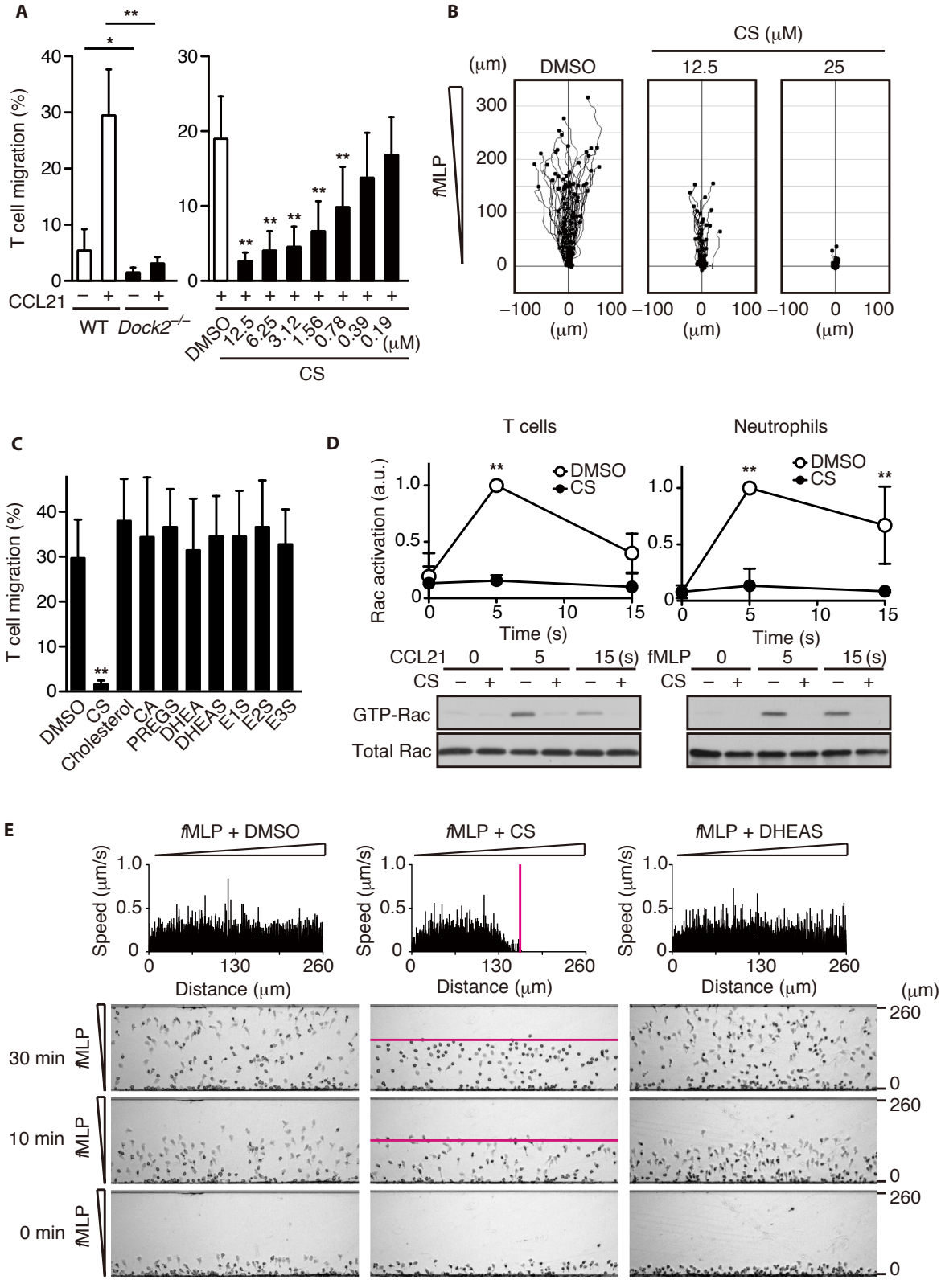

Fig. 2. CS blocks leukocyte migration by inhibiting chemoattractant-induced Rac activation. (**A**) Transwell migration assays measuring the migration of wild-type (WT) and *Dock2*$^{-/-}$ murine T cells in response to the chemoattractant CCL21 and the migration of wild-type murine T cells in response to CCL21 in the presence of the indicated concentrations of CS or vehicle only (DMSO). The percentage of T cell migration was calculated by dividing the number of T cells that migrated into the lower chamber in response to CCL21 by the number of input T cells. Data are presented as means ± SD. $n = 7$ experiments. $^{*}P < 0.05$, $^{**}P < 0.01$ (two-tailed unpaired Student's *t* test). (**B**) Migration of BM-derived murine neutrophils treated with CS or vehicle only (DMSO) along a 0 to 10 μM *f*MLP gradient over a 20-min time period. Data are representative of three independent experiments. (**C**) Migration of murine T cells in response to CCL21 in the presence of the indicated steroids. Data are presented as means ± SD. $n = 5$ to 8 experiments per treatment. $^{**}P < 0.01$ compared with control (DMSO) sample (one-way ANOVA followed by Bonferroni post hoc test). (**D**) Rac activation in murine T cells ($n = 6$ experiments) and neutrophils ($n = 5$ experiments) stimulated with CCL21 and *f*MLP, respectively, in the presence or absence of CS. Data (means ± SD) are presented as the ratio of GTP-bound Rac to total Rac after setting the 5-s value of control (DMSO) sample to an arbitrary unit (a.u.) of 1. $^{**}P < 0.01$ (two-tailed unpaired Student's *t* test). (**E**) Migration of BM-derived murine neutrophils toward a source of *f*MLP in the presence of CS, DHEAS, or vehicle only (DMSO) over a time period of 30 min. Data are representative of four independent experiments.

Downloaded from http://stke.sciencemag.org/ on August 12, 2018

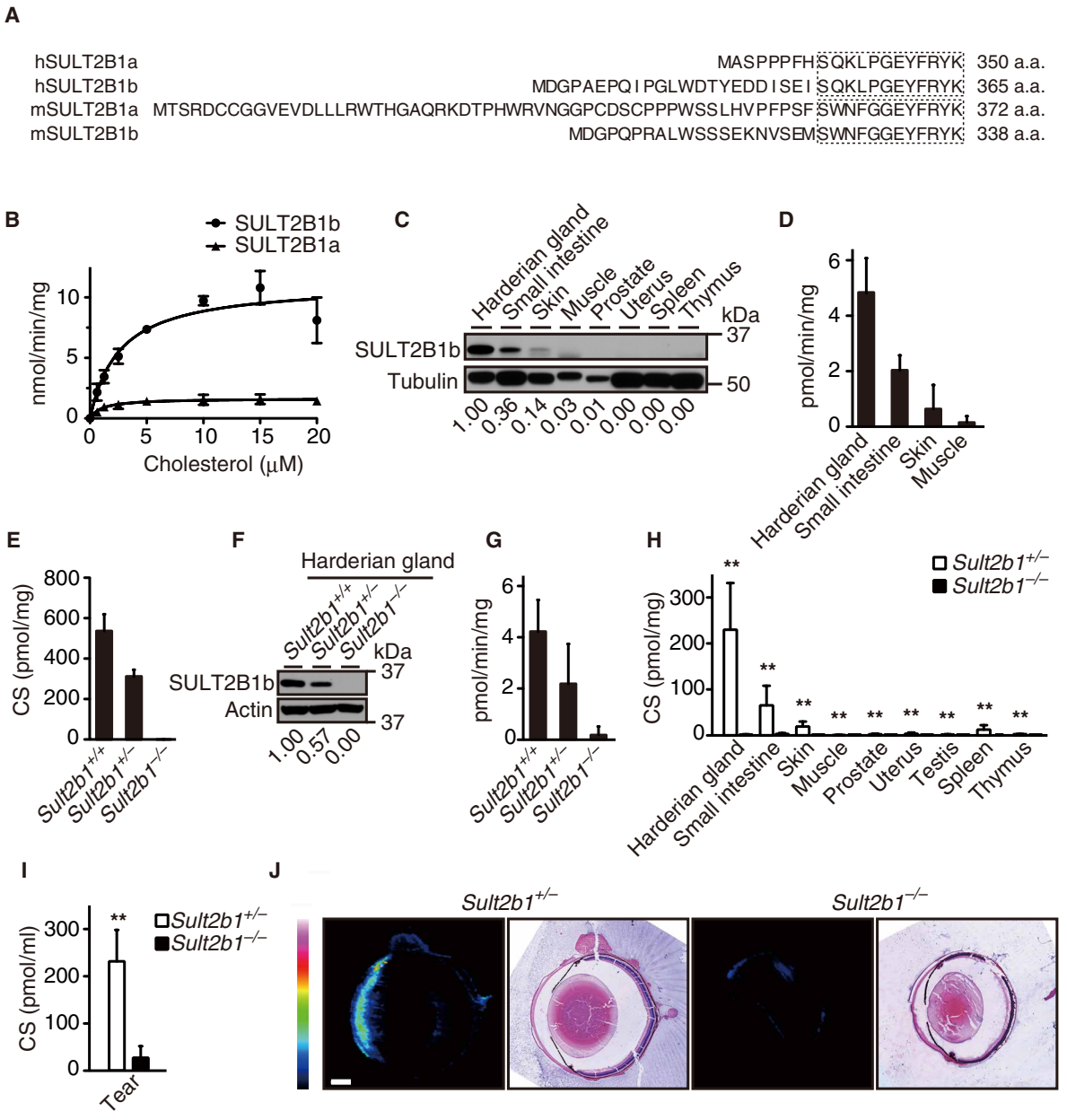

Fig. 3. CS is most abundantly produced in the Harderian gland by the sulfotransferase SULT2B1b. (**A**) Alignment of the N-terminal amino acid (a.a.) sequences of the human (h) and murine (m) SULT2B1a and SULT2B1b proteins. Conserved regions are boxed with dotted lines. (**B**) Cholesterol sulfation activity of recombinant murine SULT2B1b and SULT2B1a produced as GST fusion proteins. Assays were performed after the GST moiety was removed. Data (nanomole per minute per 1 mg of recombinant protein) are presented as means ± SD. $n = 3$ experiments. (**C**) Representative immunoblot showing SULT2B1b and tubulin in the indicated mouse tissues. The numbers below the blot indicate the abundance of SULT2B1b relative to that of tubulin in each tissue and normalized by setting the abundance of SULT2B1b in the Harderian gland as 1. Quantification data represent the means of three to five independent quantification measurements for each tissue type. (**D**) Comparison of cholesterol sulfation activity among extracts from the indicated mouse tissues. Data (picomole per minute per 1 mg of tissue lysate) are presented as means ± SD. $n = 3$ experiments. (**E**) Abundance of CS in Harderian glands from *Sult2b1*$^{+/+}$, *Sult2b1*$^{+/-}$, and *Sult2b1*$^{-/-}$ mice as quantified by liquid chromatography–tandem mass spectrometry (LC-MS/MS). Data (picomole per 1 mg of wet tissue) are presented as means ± SD. $n = 5$ glands per group. (**F**) Representative immunoblot showing SULT2B1b in Harderian glands from *Sult2b1*$^{+/+}$, *Sult2b1*$^{+/-}$, and *Sult2b1*$^{-/-}$ mice. The numbers below the blot indicate the abundance of SULT2B1b relative to actin for each tissue sample and normalized by setting the abundance of SULT2B1b in *Sult2b1*$^{+/+}$ mice as 1. Quantification data represent the mean of three experiments for each genotype. (**G**) Cholesterol sulfation activity of Harderian gland extracts from *Sult2b1*$^{+/+}$, *Sult2b1*$^{+/-}$, and *Sult2b1*$^{-/-}$ mice. Data (picomole per minute per 1 mg of tissue lysate) are presented as means ± SD. $n = 3$ experiments. (**H** and **I**) The amounts of CS in various tissues (H; $n = 7$ to 20 tissues per group; picomole per 1 mg of wet tissue) or tears (I; $n = 10$ mice per group; picomole per 1 ml of tear) from *Sult2b1*$^{+/-}$ and *Sult2b1*$^{-/-}$ mice were quantified by LC-MS/MS. Data are presented as means ± SD. $^{**}P < 0.01$ (two-tailed unpaired Student's *t* test). (**J**) Localization of CS in sections of eyeballs from *Sult2b1*$^{+/-}$ and *Sult2b1*$^{-/-}$ mice as determined by matrix-assisted laser desorption ionization (MALDI)–imaging mass spectrometry. The color bar indicates the relative intensity of the CS signal [mass/charge ratio (*m*/*z*) 465.3]. Data are representative of three independent experiments. Scale bar, 200 μm.

Downloaded from http://stke.sciencemag.org/ on August 12, 2018

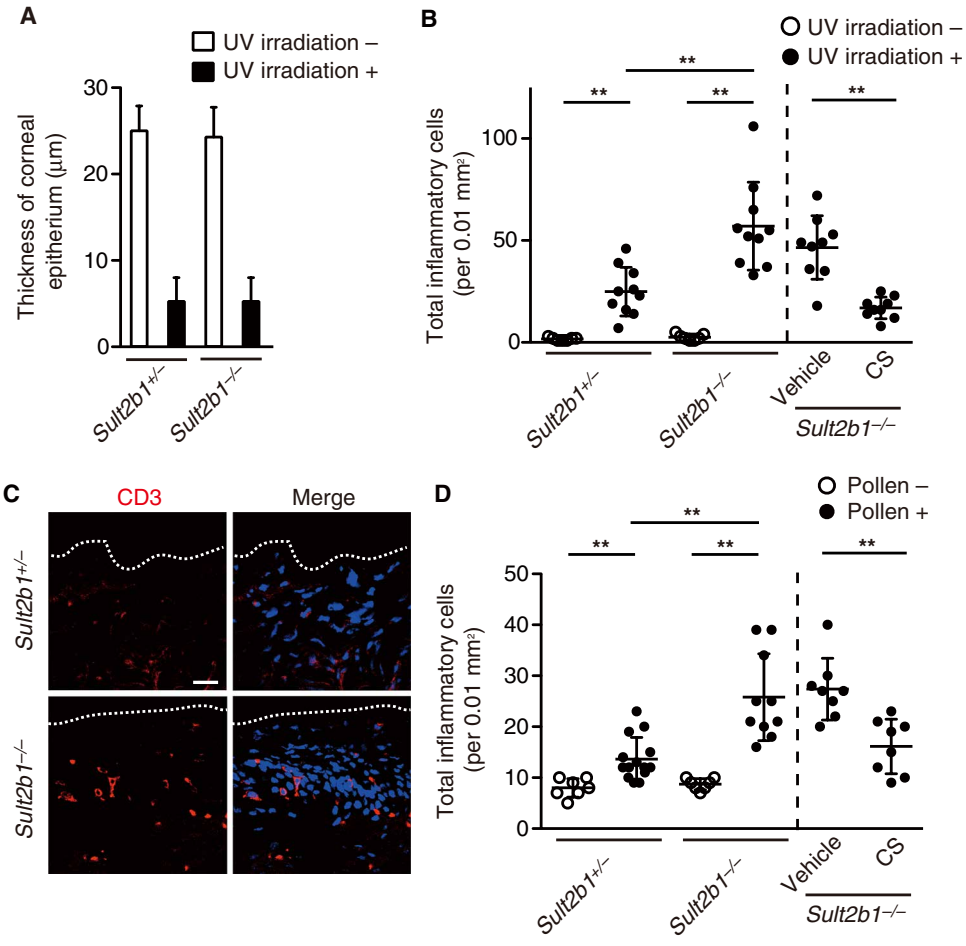

Fig. 4. CS acts locally to limit ocular surface inflammation. (**A**) Thickness of the corneal epithelium in *Sult2b1*$^{+/–}$ and *Sult2b1*$^{–/–}$ mice 24 hours after UV irradiation. Data are presented as means ± SD. $n = 7$ to 10 mice per group. (**B**) Quantification of the number of inflammatory cells in the anterior chamber of *Sult2b1*$^{+/–}$ and *Sult2b1*$^{–/–}$ photokeratitis models with (right) or without (left) CS eye drops. Data are presented as means ± SD. $n = 7$ to 10 mice per group. $^{**}P < 0.01$ (two-tailed unpaired Student's *t* test). (**C**) Immunofluorescence showing infiltration of CD3$^+$ T cells in the conjunctiva of *Sult2b1*$^{–/–}$ mice topically challenged with ragweed pollen to induce EAC. Data are representative images of seven samples per group. Scale bar, 20 μm. (**D**) Quantification of the number of inflammatory cells in the conjunctiva of *Sult2b1*$^{+/–}$ and *Sult2b1*$^{–/–}$ EAC models with (right) or without (left) CS eye drops. Data are presented as means ± SD. $n = 7$ to 14 mice per group. $^{**}P < 0.01$ (two-tailed unpaired Student's *t* test).

lymphocyte migration (fig. S9B), and its content in the Harderian gland reached only 0.0568% of that of the CS in *Sult2b1*$^{+/+}$ mice, probably because Ch25h, the enzyme responsible for the generation of 25HC (*47*), was hardly detected in the Harderian gland (fig. S10). Furthermore, both UV- and antigen-induced ocular surface inflammation were suppressed when eye drops containing CS were administered to *Sult2b1*$^{–/–}$ mice (Fig. 4, B and D). Collectively, these results indicate that CS exerts its action locally to suppress ocular surface inflammation and that exogenous CS can suppress infiltration of neutrophils and T cells to the site of inflammation.

DISCUSSION

CS has been implicated in several biological processes, yet its physiological functions are not fully understood. Here, we have identified CS as a naturally occurring DOCK2 inhibitor that binds to the catalytic DHR-2 domain and blocks its Rac GEF activity. Although CS did not affect Rac activation by Tiam1 and Trio at any concentrations tested, CS inhibited the Rac GEF activity of murine and human DOCK2 in vitro with an IC_{50} of 2.0 to 2.9 μM. This value was one order of magnitude more potent than that of 4-[3′-(2″-chlorophenyl)-2′-propen-1′-ylidene]-1-phenyl-3,5-pyrazolidinedione, which we previously developed as a small-molecule inhibitor of DOCK2 (*19*). Sulfated steroids are hydrophilic and require active transmembrane transport for cellular uptake (*32*). Although the transporter involved in CS uptake remains to be determined, CS is clearly an active inhibitor when applied to lymphocytes and neutrophils, because treatment of these cells with CS effectively inhibited DOCK2-dependent Rac activation and migration. Our results thus define a previously unknown function of CS in immune regulation.

Although *Sult2b1b* transcripts are broadly expressed in various tissues in mice (*21*, *34*, *35*), its expression in the Harderian gland has not been previously reported. By using an isoform-specific antibody, we found that SULT2B1b was highly abundant in the mouse Harderian gland. Consistent with this, CS was most abundantly produced in the Harderian gland among all tissues tested, and the concentration of CS in tears reached 231.8 nM in *Sult2b1*$^{+/–}$ mice. CS would not be necessarily required under the steady state to maintain homeostasis of the eye, because *Sult2b1*$^{–/–}$ mice kept under the specific pathogen–free condition had no indication of chronic eye inflammation. However, the lack of CS augmented UV-induced photokeratitis and antigen-induced conjunctivitis in mice, which was suppressed by CS eye drops. In humans, CS is also a normal constituent of tears and meibum (*48*), an oily substance secreted by the meibomian gland. Therefore, it is likely that CS acts locally to create environments that evade immune surveillance in the eyes of both mice and humans. So far, it has been shown that DOCK2 deficiency prevents cardiac allograft rejection and autoimmune disease development in mice (*18*, *19*). In light of these findings, CS may serve as an excellent starting place for development of DOCK2-targeting anti-inflammatory therapeutics.

MATERIALS AND METHODS

Chemical compounds

A total of 577 pharmacologically active compounds were obtained from the Drug Discovery Initiative (the University of Tokyo) and initially tested at 50 μM for their inhibitory effect on the Rac GEF activity of the DHR-2 domain of murine DOCK2. CS was purchased

Downloaded from http://stke.sciencemag.org/ on August 12, 2018

from Sigma-Aldrich (C9523) with the following steroid analogs: cholesterol (C8667), PREGS (P162), E1S (E0251), E2S (E9505), and E3S (E6375). CA (no. 151114) was purchased from Sigma-Aldrich, and DHEA (700087p), DHEAS (700086p), and 25HCS (700017p) were from Avanti. [^{3}H]-cholesterol (40 to 60 Ci/mmol) was purchased from PerkinElmer.

In vitro GEF assays

Fluorescent GEF assays were performed as described previously (*49*). Briefly, recombinant His-SUMO–tagged DOCK1 DHR-2 (mouse), DOCK2 DHR-2 (mouse and human), DOCK5 DHR-2 (mouse), Tiam DH-PH (mouse), and Trio DH-PH (mouse) proteins were produced in the Arctic BL21 (DE3) bacterial strain and purified by Ni-NTA (nitrilotriacetic acid) affinity chromatography (Qiagen). GST-fusion Rac1 was produced in BL21 (DE3) bacterial strain and purified by Glutathione Sepharose 4B chromatography (GE Healthcare). The assays consisted of GST-fusion Rac1 (10 μM), Bodipy-FL GTP (2.4 μM; Invitrogen, G12411), and GEF proteins (0.05 μM for DOCK1, 0.1 μM for DOCK2 and DOCK5, 1 μM for Trio, and 2 μM for Tiam1 depending on their GEF activities) in the reaction buffer [20 mM MES-NaOH, 150 mM NaCl, 10 mM $MgCl_2$, and 20 μM GDP (pH 7.0)] with or without steroid analogs [final concentration of DMSO, 1%]. For assays, GST-fusion Rac1 was loaded with GDP by incubating with the reaction buffer on ice for 30 min and then mixed with Bodipy-FL GTP and allowed to equilibrate at 30°C for 3 min. Recombinant GEF proteins were incubated with CS, steroid analogs, or vehicle at the indicated concentrations in the reaction buffer for 20 min at room temperature. The reaction was initiated by mixing GDP-loaded Rac1/Bodipy-FL GTP (100 μl) and GEF protein (50 μl) in a final volume of 150 μl, followed by incubating at 30°C. The change in Bodipy-FL–GTP fluorescence (excitation, 488 nm; emission, 514 nm) was monitored for 20 min using a PerkinElmer EnSpire multimode plate reader. Data were fitted using a curve fitting function of the GraphPad Prism 5 program (GraphPad Software), and the initial slope during the first 10 s was calculated (relative fluorescent unit per second) and used for comparison of the GEF activity. IC_{50} values were determined by plotting the GEF activity (percentage of control) over the log concentration of each compound and by fitting with the "log (inhibitor concentration) versus response with variable slope model" of Prism 5.

Binding assays

SPR-based binding assays were performed with a Biacore T200 instrument (GE Healthcare Life Sciences). For this purpose, His-SUMO–tagged murine DOCK2 DHR-2 protein was immobilized onto a CM5 Sensor Chip (about 7000 RUs) using an Amine Coupling Kit (GE Healthcare Life Sciences). Data were collected in Hepes-buffered saline [10 mM Hepes (pH 7.5) and 150 mM NaCl] containing 0.005% surfactant P-20, 3% DMSO, and 0.1 mM hydroxypropyl-β-cyclodextrin (HPβCD). Serial concentrations of CS were injected and binding was measured.

For steroid-binding assays, CS and various steroid analogs were dissolved in methanol (50 μl of 100 μg/ml) and were immobilized onto each well of the 96-well plates (Immulon 4HBX, Thermo Fisher Scientific) by air drying under a hood for 1 hour at room temperature. After blocking with 180 μl of tris-buffered saline [20 mM tris-HCl and 150 mM NaCl (pH 7.5)] containing 5% bovine serum albumin (BSA) for 6 hours at 4°C, each sample was incubated with 0.2 μg of His-SUMO–tagged murine DOCK2 DHR-2 protein (100 μl of 2 μg/ml) for 2.5 hours at room temperature, followed by incubation with the HisProbe horseradish peroxidase (HRP) conjugate (no. 15165, Thermo Fisher Scientific; 100 μl of 1:5000 dilution) for 1.5 hours at room temperature. The bound HRP was detected by the colorimetric assay with the 3,3′, 5,5′-tetramethylbenzidine substrate solution (no. N301, Thermo Fisher Scientific) and the stop solution (no. N600, Thermo Fisher Scientific) at an absorbance of 450 nm.

To examine the effect of CS on association between DOCK2 DHR-2 and Rac1, recombinant protein encoding His-SUMO–tagged murine DOCK2 DHR-2 domain (1 μg) was incubated with CS, steroid analogs (final 50 μM), or DMSO (2%) in 200 μl of binding buffer [20 mM MES-NaOH, 150 mM NaCl, and 2.5 mM EDTA (pH 7.0)] for 20 min at room temperature. The samples were then mixed with GST-fusion Rac1-immobilized beads (8 μl) in a total 600 μl of the binding buffer and incubated at 4°C for 1 hour on a rotating wheel. After the beads were washed twice with the binding buffer, bound proteins were separated by SDS–polyacrylamide gel electrophoresis (PAGE) and blotted with the HisProbe HRP conjugate (1:1000 dilution).

Cell preparation

Murine BM neutrophils were isolated from tibia and femur and layered onto the discontinuous Percoll (GE Healthcare) gradient. After centrifugation, cells at the 62/81% interface were recovered. Human peripheral blood samples were obtained from healthy volunteers in compliance with institutional review board protocols. Human neutrophils were prepared as described previously (*50*), and human $CD4^+$ T cells were isolated from peripheral blood mononuclear cells by magnetic sorting with Dynabeads human CD4 followed by treatment with DETACHaBEAD human CD4 (Life Technologies) (*51*). The informed consent was obtained after the nature and possible consequences of the studies were explained.

Chemotaxis assays

Transwell chemotaxis assays were performed using CCL21 as a chemoattractant for T cells. Briefly, murine splenocytes (1×10^7/ml) prepared from wild-type and *Dock2*$^{-/-}$ mice (*14*) and human $CD4^+$ T cells (1×10^6/ml) were incubated in an RPMI 1640 medium (Wako Pure Chemical Industries) containing 0.5% BSA with or without the indicated concentrations of CS, steroid analogs, or 0.2% DMSO (Transwell assay medium) at 37°C for 1 hour. Cells (1×10^6 for murine splenocytes and 1×10^5 for human $CD4^+$ T cells) were loaded into the upper chamber of the Transwells (Costar no. 3421, 5-μm pore size), which were placed onto 24-well plates containing a Transwell assay medium supplemented with CCL21 (100 to 300 ng/ml for murine splenocytes and 600 ng/ml for human $CD4^+$ T cells; both from R&D Systems). After incubation at 37°C for 6 hours (murine splenocytes) or 2 hours (human $CD4^+$ T cells), cells migrating to the lower chamber were collected and stained with a phycoerythrin (PE)–conjugated antibody for murine CD90.2 (53-2.1, BD Pharmingen) or a biotinylated antibody for human CD3 (30102X, BD Pharmingen) followed by avidin-conjugated fluorescein isothiocyanate (BD Biosciences), respectively. Flow cytometric analyses were done on FACSCalibur (BD Biosciences). The percentage of migrating T cells was calculated by dividing the number of T cells in the lower chamber by the number of input T cells.

For EZ-TAXIScan chemotaxis assays, murine BM neutrophils or human peripheral blood neutrophils were incubated in an RPMI 1640 medium containing 0.1% BSA plus CS or DMSO (0.2%) for 30 min at room temperature. Cells were then allowed to migrate along an *f*MLP gradient (0 to 10 μM; source concentration of *f*MLP = 10 μM) over the 260-μm track of an EZ-TAXIScan chamber (Effector Cell

Downloaded from http://stke.sciencemag.org/ on August 12, 2018

Institute) at 37°C. In some assays, murine BM neutrophils were allowed to migrate toward the *f*MLP source (3 μM) containing CS, DHEAS (150 μM), or vehicle (3% DMSO). Phase-contrast image of migrating cells were acquired at 30-s intervals for 30 min. Images were imported as stacks to the ImageJ program (National Institutes of Health) and analyzed with the manual tracking and the chemotaxis and migration tools.

Rac activation assays

To examine the effect of CS on Rac activation, murine T cells or BM neutrophils were treated in Hanks' balanced salt solution (Invitrogen) with CS (100 μM) or DMSO (0.2%) alone for 30 min. Immediately after stimulation with CCL21 (1 μg/ml) or *f*MLP (10 μM), cells were lysed by adding 1× Mg^{2+} lysis buffer [MLB; 25 mM Hepes (pH 7.5), 150 mM NaCl, 1% Igepal CA-630, 10 mM $MgCl_2$, 1 mM EDTA, and 10% glycerol; Millipore), followed by centrifugation at 20,000*g* for 1 min at 4°C. Aliquots were saved for total cell lysate controls, and the remaining lysates were incubated with agarose beads containing the GST-fusion Rac-binding domain of PAK1 (no. 14-325, Millipore) at 4°C for 1 hour. The beads were washed twice with 1× MLB buffer and suspended in SDS-PAGE sample buffer [62.5 mM tris-HCl (pH 6.8), 2% SDS, 10% glycerol, 0.005% bromophenol blue, and 2.5% 2-mercaptoethanol]. The bound proteins and total cell lysates were separated by SDS-PAGE on a 12.5% polyacrylamide gel, and blots were probed with a monoclonal antibody for Rac1 (23A8, 1:2000 dilution; Millipore).

Mice

Sult2b1$^{-/-}$ mice, which were generated by using a targeting vector to replace exons 3 to 7 of the *Sult2b1* gene with an angiotensin-converting enzyme–Cre–neomycin (ACN) cassette (*52*), have been described previously (*30*, *38*) and were obtained from the Jackson Laboratory (stock no. 018773). Mice heterozygous for the mutant allele (*Sult2b1*$^{+/-}$) were backcrossed with C57BL/6 mice (purchased from Japan Clea) for more than five generations, and age- and sex-matched *Sult2b1*$^{+/-}$ and *Sult2b1*$^{-/-}$ littermates were analyzed in functional assays. Mice were maintained under specific pathogen–free conditions in the animal facility of Kyushu University. The protocol of animal experiments was approved by the committee of Ethics on Animal Experiments of Kyushu University.

Genotyping polymerase chain reaction and Southern blot analysis

Genotyping polymerase chain reaction (PCR) was performed using the KOD FX DNA polymerase (TOYOBO) and the following primers: s1, 5′-GACAGCGCAGGGCCACAC-3′; s2, 5′-CTTATTCAACCACCACACCCAT-3′; and as1, 5′-TCCATCCCTAGCTTCACATGG-3′. Amplified products for wild-type allele and KO allele were 215 bp (s1 and as1) and 469 bp (s2 and as1), respectively. For Southern blot analysis, genomic DNA was isolated from the tail of each mouse, digested with Eco RI and Eco RV, separated on a 1% agarose gel, and transferred onto the Hybond-XL nylon membrane (GE Healthcare) by the alkaline transfer method. DNA fragments of 0.5 kb covering the exons 4 and 5 and 0.25 kb carrying a portion of the intron 2 were labeled with [α-32P]-dCTP (3000 Ci/mmol, PerkinElmer) using the Megaprime DNA labeling system (RPN1606, GE Healthcare) and were used as a probe for hybridization in the hybridization buffer [50% formamide, 5× SSPE, 5× Denhardt's solution, 1% SDS, and salmon sperm DNA (100 μg/ml)]. After washing, the hybridized membrane was analyzed by BAS-2500 bio-imaging analyzer.

SULT assays

The complementary DNAs encoding murine SULT2B1a and SULT2B1b were cloned in the Eco RI–Xho I sites of the pGEX 6P-1 vector (GE Healthcare) and the pET-SUMO vector. GST-fusion SULT2B1a and SULT2B1b were produced in BL21 (DE3) bacterial strain and purified by Glutathione Sepharose 4B chromatography (GE Healthcare). The GST moiety was removed by cleavage with PreScission Protease (no. 27084301, GE Healthcare). His-SUMO–tagged SULT2B1b was produced in the Arctic BL21 (DE3) bacterial strain and purified by Ni-NTA affinity chromatography (Qiagen). The His-SUMO moiety was removed by cleavage with SUMO protease 1 (no. 4010, LifeSensors). The N-terminal amino acid sequence was determined by Edman degradation. At the N terminus, the GST-cleaved SULT2B1a/SULT2B1b and His-SUMO–cleaved SULT2B1b contained the following vector-derived extra peptides: GPLGSPEF and EHLYFQGSEF, respectively.

SULT activity was determined using radiolabeled cholesterol as described (*36*, *37*) with slight modifications. For the kinetic analyses, 0.31 μg of SULT2B1a or 0.15 μg of SULT2B1b protein was used in the reaction mixture (50 μl) consisting of 0 to 20 μM [^{3}H]-cholesterol (~1500 dpm/pmol), 0.1 mM 3′-phosphoadenosine 5′-phosphosulfate (PAPS; Sigma-Aldrich, A1651) in 10 mM tris-HCl (pH 7.5) containing 5 mM $MgCl_2$, 0.2 mM HPβCD, and 5% ethanol (v/v). Reactions were initiated by adding 2 mM PAPS (2.5 μl), carried out at 37°C for 10 min, and terminated by adding 0.8 ml of ethanol. Samples were frozen at −20°C for 60 min, followed by centrifugation at 20,000*g* for 5 min at 4°C to remove precipitates. The supernatant was recovered in a fresh tube, evaporated using the SpeedVac (no. SPD1010, Thermo Fisher Scientific), redissolved in 8 μl of methanol containing 16 μg of CS as a carrier, and applied to a thin-layer chromatography (TLC) sheet (Chromato Sheet II, Wako, 038-24061), which was developed using a solvent system consisting of chloroform/acetone/methanol/acetic acid/water (8:4:2:2:1). After drying, the TLC sheet was developed by exposure to I_2 vapor. CS spots were excised, and the radioactivity was determined by the liquid scintillation counter.

For determination of tissue SULT activity, tissues were isolated, suspended in 300 μl of ice-cold phosphate-buffered saline (PBS)/water (1:1) supplemented with 1 mM dithiothreitol and protease inhibitor cocktail (cOmplete, Roche), and homogenized using the POLYTRON homogenizer (PT 1200E, KINEMATICA AG), followed by centrifugation at 20,000*g* for 30 min at 4°C. The supernatant was recovered and clarified using the Millex-LH 0.45-μm filter (Millipore) to obtain tissue lysates. The reaction mixture (50 μl) consisted of the tissue lysates (2 to 10 μg of protein), 10 μM [^{3}H]-cholesterol (~2800 dpm/pmol), 0.1 mM PAPS in 10 mM tris-HCl (pH 7.5) containing 5 mM $MgCl_2$, 0.2 mM HPβCD, and 3.5% ethanol (v/v). Reactions were initiated by adding 2 mM PAPS (2.5 μl), carried out at 37°C for 30 min, and terminated by adding 0.8 ml of ethanol. Samples were processed as described above, and the radioactivity was determined by the liquid scintillation counter.

Western blot analyses for SULT2B1b abundance

To examine the abundance of SULT2B1b in each tissue, polyclonal antibody that specifically recognizes murine SULT2B1b was produced by immunizing rabbits with keyhole limpet hemocyanin (KLH)–coupled synthetic peptide corresponding to the N-terminal sequence of SULT2B1b with additional cysteine for coupling (MDGPQPRALWSSSEKNVSEMSWNC). A polyclonal antibody that recognizes both murine SULT2B1a and SULT2B1b was produced by immunizing rabbits with a KLH-coupled synthetic peptide corresponding to the

Downloaded from http://stke.sciencemag.org/ on August 12, 2018

C-terminal conserved sequence with additional cysteine for coupling (CSPSPASDDPNPG). In some experiments, human embryonic kidney 293T cells were transfected by polyethylenimine with pMX–internal ribosomal entry site–green fluorescent protein vectors encoding murine SULT2B1b, its mutant lacking N-terminal 23–amino acid residues (ΔN) or SULT2B1a with or without C-terminal hemagglutinin (HA) tag, and their lysates were used as controls. Freshly isolated tissues were homogenized in a 15-ml polypropylene tube containing 1 ml of lysis buffer [20 mM tris-HCl (pH 7.5), 150 mM NaCl, 1 mM EDTA, 1 mM EGTA, 1% Triton X-100, 2.5 mM sodium pyrophosphate, 1 mM β-glycerophosphate, and 1 mM sodium vanadate] supplemented with 5× protease inhibitor cocktail (cOmplete, Roche) using the homogenizer (Ultra-Turrax T8, IKA-Werke) set at dial 4 for 1 min on ice. The homogenates were transferred to 1.5-ml tubes and centrifuged at 20,000*g* at 4°C for 5 min. After centrifugation, the supernatants were mixed with an equal volume of 2× sample buffer [125 mM tris-HCl (pH 6.8), 4% SDS, 20% glycerol, 0.01% bromophenol blue, and 5% 2-mercaptoethanol] and boiled for 5 min. Total protein concentration was measured by the DC Protein Assay Reagent (Bio-Rad). Tissue or cell extracts (20 μg per lane) were separated by SDS-PAGE and immunoblotted with a rabbit antibody for SULT2B1b (1:1000 dilution), rabbit antibody for SULT2B1a/1b (1:1000 dilution), goat antibody for actin (I-19, 1:1000 dilution; Santa Cruz Biotechnology), rabbit monoclonal antibody for β-tubulin (9F3, 1:1000 dilution; Cell Signaling Technology), or rat monoclonal antibody for HA (3F10, 1:2000 dilution; Roche), followed by incubation with HRP-conjugated secondary antibodies.

Quantification of CS by mass spectrometry

For sample preparation, tissues were freshly isolated from mice, quickly frozen with liquid nitrogen, and stored at −80°C until analyses. Frozen samples were mixed with an internal standard (IS) compound (deuterium-labeled CS; d7-CS), and homogenized in ice-cold methanol (500 μl) using a homogenizer (Finger Masher AM79330; Sarstedt). The supernatant was filtered using the ultrafiltration devices (UltrafreeMC-PLHCC; Human Metabolome Technologies), and the filtrate was directly analyzed by LC-MS/MS for CS content. Tear fluid was collected using a microglass capillary tube (Microcap no. 1-000-0005, Drummond), mixed with 10 μl of methanol containing IS, and concentrated with a vacuum concentrator (SpeedVac; Thermo Fisher Scientific). Samples collected at less than 0.2 μl were omitted from the analyses. The concentrates were dissolved in 15 μl of methanol and analyzed by LC-MS/MS.

For quantification of CS with LC-MS/MS, a triple-quadrupole mass spectrometer equipped with an electrospray ionization (ESI) ion source (LCMS-8040; Shimadzu Corporation) was used in the negative-ESI and multiple reaction monitoring modes. The samples were resolved on the Mastro-C18 column (2.1 mm × 100 mm, 3-μm particle, Shimadzu GLC) by isocratic flow with mobile phase A (200 mM ammonium acetate) and mobile phase B (methanol) at ratios of 1:9 and a flow rate of 0.4 ml/min, with a column temperature of 40°C. CS and IS (d7-CS) signals were monitored by ion transitions at m/z 465.3 > 97 and 472.3 > 97, respectively. The absolute content of CS was calculated by using peak area ratios of CS against IS. For quantification of 25HCS content, the signal of ion transition at m/z 481.3 > 97 was monitored, and the peak area of 25HCS was quantified and calculated relative to that of CS.

MALDI-imaging mass spectrometry

MALDI-imaging analyses were performed as described previously (*53*, *54*). Briefly, thin sections (8 μm) of the eye and the Harderian gland were prepared with a cryomicrotome (CM3050, Leica Microsystems) and a Kawamoto cryofilm to support the fragile eyeball tissues during cutting. Tissue sections were mounted onto indium tin oxide–coated glass slides (Bruker Daltonics). Eyeball sections on the Kawamoto cryofilm were attached with electrically conducting double-adhesive tape (Shimadzu Corporation). These sections were coated with 9-aminoacridine as the matrix (10 mg/ml; dissolved in 80% ethanol) by manually spraying with an artistic brush (Procon Boy FWA Platinum, Mr. Hobby). The matrix was simultaneously applied to the multiple sections to maintain consistent analyte extraction and cocrystallization conditions. MALDI imaging was performed using an Ultraflextreme MALDI–time-of-flight (TOF)/TOF mass spectrometer and 7T Fourier transform ion cyclotron resonance mass spectrometry (FT-ICR-MS; Solarix Bruker Daltonics) equipped with an yttrium-aluminum-garnet–Nd laser. Data were acquired in the negative reflectron mode with raster scanning by a pitch distance of 50 μm. Each spectrum was the result of 300 laser shots at each data point. In the TOF/TOF measurement, signals between m/z 50 and 1000 were collected. In the FT-ICR-MS imaging, signals between m/z 300 and 500 were collected by using continuous accumulation of selected ion mode. Image reconstruction for both was performed using FlexImaging 4.1 software (Bruker Daltonics). Molecular identification was done by FT-ICR-MS data; the high mass accuracy provided by FT-ICR-MS allowed selective ion signals for the metabolites to be obtained within a mass window of 5 parts per million, enabling to identify the specific elemental composition of compounds by querying the highly accurate masses against database (*55*).

Disease models for ocular surface inflammation

Photokeratitis was induced as previously described (*39*). Briefly, mice were irradiated with UVB at 100 mJ cm^{-2} s^{-1} for 100 s using a spot light source (LIGHTNING CURE Spot light source LC8 L9588-02, Hamamatsu Photonics) under anesthesia. The spectral irradiance for the UV lamps was 280 to 400 nm, and the UVB output was monitored by a Digital UV meter (280 to 320 nm, Solarmeter). After 24 hours, the eyes were harvested for histological examinations. For induction of EAC, mice were immunized with 50 μg of SRW pollen (Greer Laboratories) in 5 mg of Imject Alum Adjuvant (77161, Thermo Fisher Scientific) into footpads on day 0 (*42*). Ten days later, 1.5 mg of SRW pollen suspended in 10 μl of PBS was topically administered into each eye once a day for 3 days. On day 13, 24 hours after the last pollen application, the eyes were harvested for histological examinations.

Histological analyses were performed as follows. The eyes were fixed in 4% glutaraldehyde in PBS for 1 hour at room temperature and then fixed in 10% paraformaldehyde in PBS overnight. After being embedded in paraffin, tissues sections (5 μm thick) were cut through the papillary–optic nerve plane and were stained with hematoxylin and eosin. The number of inflammatory cells per 0.01 mm^2 was counted. For immunofluorescence analyses, the eyes were embedded in optimal cutting temperature compound (Sakura Finetek) and frozen in liquid nitrogen. Cryostat sections (5 μm thick) were fixed in 4% paraformaldehyde for 30 min and blocked with 1% BSA in PBS for 1 hour at room temperature. Sections were then stained with PE-conjugated antibody for murine CD3 (17A2, 4 μg/ml; BioLegend), biotinylated antibody for murine CD45R (RA3-6B2, 5 μg/ml; BD Biosciences), or biotinylated antibody for murine Gr1 (Ly6G/Ly6C) (RB6-8C5, 5 μg/ml; BD Biosciences) followed by incubation with Alexa Fluor 546–conjugated streptavidin

Downloaded from http://stke.sciencemag.org/ on August 12, 2018

(4 μg/ml; Thermo Fisher Scientific). All images were obtained with a laser scanning confocal microscope (Carl Zeiss). The investigators who performed the experiments were not blinded to mouse genotypes.

CS-containing eye drops

CS was dissolved in 40 mM HPβCD before use. In UV-induced photokeratitis models, 10 μl of CS (8 μg/μl) or vehicle only (40 mM HPβCD) was administered topically to the eye of *Sult2b1*$^{-/-}$ mice for a total of six times: once 5 min before irradiation and five times subsequently at 4-hour intervals. In EAC models, 10 μl of CS (8 μg/μl) or vehicle (40 mM HPβCD) was administered topically to the eye of *Sult2b1*$^{-/-}$ mice three times per day at 4-hour intervals on days 10, 11, and 12.

Reverse transcription PCR

Total RNA was isolated from tissues using ISOGEN (Nippon Gene). After treatment with ribonuclease-free deoxyribonuclease I (Life Technologies), RNA samples were reverse-transcribed with oligo(dT) primers (Life Technologies) and SuperScript III reverse transcriptase (Life Technologies) for amplification by PCR. Real-time PCR was performed on a CFX Connect Real Time System (Bio-Rad) using the SYBR Green PCR Master Mix (Applied Biosystems). The following PCR primers were used: for *Gapdh*, 5′-TGTGTCCGTCGTGGATCTGA-3′ and 5′-TTGCTGTTGAAGTCGCAGGAG-3′; and for *Ch25h*, the commercial validated primers #qMmuCED0001765 (Bio-Rad).

Statistical analyses

Statistical analyses were performed using GraphPad Prism. The data were initially tested with a Kolmogorov-Smirnov test for normal distribution. Parametric data were analyzed using a two-tailed unpaired Student's *t* test when two groups were compared or a one-way ANOVA followed by Bonferroni post hoc test when multiple groups were compared. Nonparametric data were analyzed with a Mann-Whitney test when two groups were compared. $P < 0.05$ was considered significant.

SUPPLEMENTARY MATERIALS

www.sciencesignaling.org/cgi/content/full/11/541/eaao4874/DC1
Fig. S1. CS inhibits the Rac GEF activity of murine and human DOCK2.
Fig. S2. CS blocks human leukocyte migration.
Fig. S3. Cholesterol sulfation activity of recombinant murine SULT2B1b expressed as a His-SUMO–tagged protein.
Fig. S4. Validation of the antibody used to detect murine SULT2B1b.
Fig. S5. Validation of the antibody used to detect murine SULT2B1a and SULT2B1b.
Fig. S6. Generation and genotyping of *Sult2b1*$^{-/-}$ mice.
Fig. S7. Mass spectrometry imaging of CS in the Harderian glands from *Sult2b1*$^{+/-}$ and *Sult2b1*$^{-/-}$ mice.
Fig. S8. Infiltration of Gr1^{+} neutrophils into the anterior chamber in UV-induced photokeratitis model.
Fig. S9. 25HCS treatment does not affect migration of murine T cells.
Fig. S10. *Ch25h* is barely expressed in the Harderian gland.
Movie S1. CS halts chemotaxis of murine neutrophils.

REFERENCES AND NOTES

1. E. Kolaczkowska, P. Kubes, Neutrophil recruitment and function in health and inflammation. *Nat. Rev. Immunol.* **13**, 159–175 (2013).
2. C. Munz, J. D. Lunemann, M. T. Getts, S. D. Miller, Antiviral immune responses: Triggers of or triggered by autoimmunity? *Nat. Rev. Immunol.* **9**, 246–258 (2009).
3. J. Y. Niederkorn, See no evil, hear no evil, do no evil: The lessons of immune privilege. *Nat. Immunol.* **7**, 354–359 (2006).
4. J. V. Forrester, H. Xu, T. Lambe, R. Cornall, Immune privilege or privileged immunity? *Mucosal Immunol.* **1**, 372–381 (2008).
5. A. L. Mellor, D. H. Munn, Creating immune privilege: Active local suppression that benefits friends, but protects foes. *Nat. Rev. Immunol.* **8**, 74–80 (2008).
6. J. A. Joyce, D. T. Fearon, T cell exclusion, immune privilege, and the tumor microenvironment. *Science* **348**, 74–80 (2015).
7. A. L. Mellor, D. H. Munn, IDO expression by dendritic cells: Tolerance and tryptophan catabolism. *Nat. Rev. Immunol.* **4**, 762–774 (2004).
8. V. Bronte, P. Zanovello, Regulation of immune responses by L-arginine metabolism. *Nat. Rev. Immunol.* **5**, 641–654 (2005).
9. T. A. Ferguson, T. S. Griffith, A vision of cell death: Fas ligand and immune privilege 10 years later. *Immunol. Rev.* **213**, 228–238 (2006).
10. T. Okazaki, T. Honjo, The PD-1–PD-L pathway in immunological tolerance. *Trends Immunol.* **27**, 195–201 (2006).
11. K. Reif, J. G. Cyster, The CDM protein DOCK2 in lymphocyte migration. *Trends Cell Biol.* **12**, 368–373 (2002).
12. J.-F. Côté, K. Vuori, Identification of an evolutionarily conserved superfamily of DOCK180-related proteins with guanine nucleotide exchange activity. *J. Cell Sci.* **115**, 4901–4913 (2002).
13. K. Kulkarri, J. Yang, Z. Zhang, D. Barford, Multiple factors confer specific Cdc42 and Rac protein activation by dedicator of cytokinesis (DOCK) nucleotide exchange factors. *J. Biol. Chem.* **286**, 25341–25351 (2011).
14. Y. Fukui, O. Hashimoto, T. Sanui, T. Oono, H. Koga, M. Abe, A. Inayoshi, M. Noda, M. Oike, T. Shirai, T. Sasazuki, Haematopoietic cell-specific CDM family protein DOCK2 is essential for lymphocyte migration. *Nature* **412**, 826–831 (2001).
15. T. Sanui, A. Inayoshi, M. Noda, E. Iwata, M. Oike, T. Sasazuki, Y. Fukui, DOCK2 is essential for antigen-induced translocation of TCR and lipid rafts, but not PKC-θ and LFA-1, in T cells. *Immunity* **19**, 119–129 (2003).
16. Y. Kunisaki, A. Nishikimi, Y. Tanaka, R. Takii, M. Noda, A. Inayoshi, K.-i. Watanabe, F. Sanematsu, T. Sasazuki, T. Sasaki, Y. Fukui, DOCK2 is a Rac activator that regulates motility and polarity during neutrophil chemotaxis. *J. Cell Biol.* **174**, 647–652 (2006).
17. Y. Sakai, Y. Tanaka, T. Yanagihara, M. Watanabe, X. Duan, M. Terasawa, A. Nishikimi, F. Sanematsu, Y. Fukui, The Rac activator DOCK2 regulates natural killer cell–mediated cytotoxicity in mice through the lytic synapse formation. *Blood* **18**, 386–393 (2013).
18. H. Jiang, F. Pan, L. M. Erickson, M.-S. Jang, T. Sanui, Y. Kunisai, T. Sasazuki, M. Kobayashi, Y. Fukui, Deletion of DOCK2, a regulator of the actin cytoskeleton in lymphocytes, suppresses cardiac allograft rejection. *J. Exp. Med.* **202**, 1121–1130 (2005).
19. A. Nishikimi, T. Uruno, X. Duan, Q. Cao, Y. Okamura, T. Saitoh, N. Saito, S. Sakaoka, Y. Du, A. Suenaga, M. Kukimoto-Niino, K. Miyano, K. Gotoh, T. Okabe, F. Sanematsu, Y. Tanaka, H. Sumimoto, T. Honma, S. Yokoyama, T. Nagano, D. Kohda, M. Kanai, Y. Fukui, Blockade of inflammatory responses by a small-molecule inhibitor of the Rac activator DOCK2. *Chem. Biol.* **19**, 488–497 (2012).
20. K. Dobbs, C. Domínguez Conde, S.-Y. Zhang, S. Parolini, M. Audry, J. Chou, E. Haapaniemi, S. Keles, I. Bilic, S. Okada, M. J. Massaad, S. Rounioja, A. M. Alwahadneh, N. K. Serwas, K. Capuder, E. Çiftçi, K. Felgentreff, T. K. Ohsumi, V. Pedergnana, B. Boisson, Ş. Haskoloğlu, A. Ensari, M. Schuster, A. Moretta, Y. Itan, O. Patrizi, F. Rozenberg, P. Lebon, J. Saarela, M. Knip, S. Petrovski, D.B. Goldstein, R. E. Parrott, B. Savas, A. Schambach, G. Tabellini, C. Bock, T. A. Chatila, A. M. Comeau, R. S. Geha, L. Abel, R. H. Buckley, A. İkincioğulları, W. Al-Herz, M. Helminen, F. Doğu, J.-L. Casanova, K. Boztuğ, L. D. Notarangelo, Inherited DOCK2 deficiency in patients with early-onset invasive infections. *N. Engl. J. Med.* **372**, 2409–2422 (2015).
21. C. A. Strott, Y. Higashi, Cholesterol sulfate in human physiology: What's it all about? *J. Lipid Res.* **44**, 1268–1278 (2003).
22. A. M. Jetten, M. A. George, C. Nervi, L. R. Boone, J. I. Rearick, Increased cholesterol sulfate and cholesterol sulfotransferase activity in relation to the multi-step process of differentiation in human epidermal keratinocytes. *J. Invest. Dermatol.* **92**, 203–209 (1989).
23. Y. Higashi, H. Fuda, H. Yanai, Y. Lee, T. Fukushige, T. Kanzaki, C. A. Strott, Expression of cholesterol sulfotransferase (SULT2B1b) in human skin and primary cultures of human epidermal keratinocytes. *J. Invest. Dermatol.* **122**, 1207–1213 (2004).
24. M. Shimada, T. Matsuda, A. Sato, T. Matsubara, K. Nagata, Y. Yamazoe, Expression of a skin cholesterol sulfotransferase, St2b2, is a trigger of epidermal cell differentiation. *Xenobiotica* **38**, 1487–1499 (2008).
25. O. Hanyu, H. Nakae, T. Miida, Y. Higashi, H. Fuda, M. Endo, A. Kohjitani, H. Sone, C. A. Strott, Cholesterol sulfate induces expression of the skin barrier protein filaggrin in normal human epidermal keratinocytes through induction of RORα. *Biochem. Biophys. Res. Commun.* **428**, 99–104 (2012).
26. J. Langlais, M. Zollinger, L. Plante, A. Chapdelaine, G. Bleau, K. D. Roberts, Localization of cholesteryl sulfate in human spermatozoa in support of a hypothesis for the mechanism of capacitation. *Proc. Natl. Acad. Sci. U.S.A.* **78**, 7266–7270 (1981).
27. M. Merten, J. F. Dong, J. A. Lopez, P. Thiagarajan, Cholesterol sulfate. A new adhesive molecule for platelets. *Circulation* **103**, 2032–2034 (2001).
28. T. Shimada, H. Kato, S. Iwanaga, M. Iwamori, Y. Nagai, Activation of factor XII and prekallikrein with cholesterol sulfate. *Thromb. Res.* **38**, 21–31 (1985).
29. D. A. Aleksandrov, A. N. Zagryagskaya, M. A. Pushkareva, M. Bachschmid, M. Peters-Golden, O. Werz, D. Steinhilber, G. F. Sud'ina, Cholesterol and its anionic

Downloaded from http://stke.sciencemag.org/ on August 12, 2018

derivatives inhibit 5-lipoxygenase activation in polymorphonuclear leukocytes and MonoMac6 cells. *FEBS J.* **273**, 548–557 (2006).
30. F. Wang, K. Beck-García, C. Zorzin, W. W. A. Schamel, M. M. Davis, Inhibition of T cell receptor signaling by cholesterol sulfate, a naturally occurring derivative of membrane cholesterol. *Nat. Immunol.* **17**, 844–850 (2016).
31. A. P. Payne, The Harderian gland: A tercentennial review. *J. Anat.* **185**, 1–49 (1994).
32. J. W. Mueller, L. C. Gilligan, J. Idkowiak, W. Arlt, P. A. Foster, The regulation of steroid action by sulfation and desulfation. *Endocr. Rev.* **36**, 526–563 (2015).
33. C. N. Falany, D. He, N. Dumas, A. R. Frost, J. L. Falany, Human cytosolic sulfotransferase 2B1: Isoform expression, tissue specificity and subcellular localization. *J. Steroid Biochem. Mol. Biol.* **102**, 214–221 (2006).
34. C. Shimizu, H. Fuda, H. Yanai, C. A. Strott, Conversion of the hydroxysteroid sulfotransferase *SULT2B1* gene structure in the mouse: Pre- and postnatal expression, kinetics analysis of isoforms, and comparison with prototypical SULT2A1. *Endocrinology* **144**, 1186–1193 (2003).
35. C. N. Falany, K. J. Rohn-Glowacki, SULT2B1: Unique properties and characteristics of a hydroxysteroid sulfotransferase family. *Drug Metab. Rev.* **45**, 388–400 (2013).
36. H. Fuda, Y. C. Lee, C. Shimizu, N. B. Javitt, C. A. Strott, Mutational analysis of human hydroxysteroid sulfotransferase SULT2B1 isoforms reveals that exon 1B of the *SULT2B1* gene produces cholesterol sulfotransferase, whereas exon 1A yields pregnenolone sulfotransferase. *J. Biol. Chem.* **277**, 36161–36166 (2002).
37. C. A. Meloche, C. N. Falany, Expression and characterization of the human 3 beta-hydroxysteroid sulfotransferases (SULT2B1a and SULT2B1b). *J. Steroid Biochem. Mol. Biol.* **77**, 261–269 (2001).
38. B. Dong, P. K. Saha, W. Huang, W. Chen, L. A. Abu-Elheiga, S.-J. Wakil, R. D. Stevens, O. Ilkayeva, C. B. Newgard, L. Chan, D. D. Moore, Activation of nuclear receptor CAR ameliorates diabetes and fatty liver disease. *Proc. Natl. Acad. Sci. U.S.A.* **106**, 18831–18836 (2009).
39. N. Kitaichi, T. Shimizu, K. Yoshida, A. Honda, Y. Yoshihisa, S. Kase, K. Ohgami, O. Norisugi, T. Makino, J. Nishihira, S. Yamagishi, S. Ohno, Macrophage migration inhibitory factor ameliorates UV-induced photokeratitis in mice. *Exp. Eye Res.* **86**, 929–935 (2008).
40. M. V. Riley, S. A. Elgebaly, The release of a neutrophil chemotactic factor from UV-B irradiated corneas in vitro. *Curr. Eye Res.* **9**, 677–682 (1990).
41. Y. C. Shao, J. C. Liou, C. Y. Kuo, Y. S. Tsai, E. C. Lin, C. J. Hsieh, S. P. Lin, B. Y. Chen, UVB promotes the initiation of uveitic inflammatory injury in vivo and is attenuated by UV-blocking protection. *Mol. Vis.* **23**, 219–227 (2017).
42. D.-Q. Li, L. Zhang, S. C. Pflugfelder, C. S. De Paiva, X. Zhang, G. Zhao, X. Zheng, Z. Su, Y. Qu, Short ragweed pollen triggers allergic inflammation through Toll-like receptor 4-dependent thymic stromal lymphopoietin/OX40 ligand/OX40 signaling pathways. *J. Allergy Clin. Immunol.* **128**, 1318–1325.e2 (2011).
43. N. B. Javitt, Y. C. Lee, C. Shimizu, H. Fuda, C. A. Strott, Cholesterol and hydroxycholesterol sulfotransferase: Identification, distinction from dehydroepiandrosterone sulfotransferase, and differential tissue expression. *Endocrinology* **142**, 2978–2984 (2001).
44. H. Fuda, N. B. Javitt, K. Mitamura, S. Ikegawa, C. A. Strott, Oxysterols are substrates for cholesterol sulfotransferase. *J. Lipid Res.* **48**, 1343–1352 (2007).
45. X. Li, W. M. Pandak, S. K. Erickson, Y. Ma, L. Yin, P. Hylemon, S. Ren, Biosynthesis of the regulatory oxysterol, 5-cholesten-3β,25-diol 3-sulfate, in hepatocytes. *J. Lipid Res.* **48**, 2587–2596 (2007).
46. L. Xu, Q. Bai, D. Rodriguez-Agudo, P. B. Hylemon, D. M. Heuman, W. M. Pandak, S. Ren, Regulation of hepatocytes lipid metabolism and inflammatory response by 25-hydroxycholesterol and 25-hydroxycholesterol-3-sulfate. *Lipids* **45**, 821–832 (2010).
47. E. G. Lund, T. A. Kerr, J. Sakai, W.-P. Li, D. W. Russell, cDNA cloning of mouse and human cholesterol 25-hydroxylases, polytopic membrane proteins that synthesize a potent oxysterol regulator of lipid metabolism. *J. Biol. Chem.* **273**, 34316–34327 (1998).
48. S. M. Lam, L. Tong, X. Duan, A. Petznick, M. R. Wenk, G. Shui, Extensive characterization of human tear fluid collected using different techniques unravels the presence of novel lipid amphiphiles. *J. Lipid Res.* **55**, 289–298 (2014).
49. H. Tajiri, T. Uruno, T. Shirai, D. Takaya, S. Matsunaga, D. Setoyama, M. Watanabe, M. Kukimoto-Niino, K. Oisaki, M. Ushijima, F. Sanematsu, T. Honma, T. Terada, E. Oki, S. Shirasawa, Y. Maehara, D. Kang, J.-F. Côté, S. Yokoyama, M. Kanai, Y. Fukui, Targeting Ras-driven cancer cell survival and invasion through selective inhibition of DOCK1. *Cell Rep.* **19**, 969–980 (2017).
50. M. Watanabe, M. Terasawa, K. Miyano, T. Yanagihara, T. Uruno, F. Sanematsu, A. Nishikimi, J.-F. Côté, H. Sumimoto, Y. Fukui, DOCK2 and DOCK5 act additively in neutrophils to regulate chemotaxis, superoxide production, and extracellular trap formation. *J. Immunol.* **193**, 5660–5667 (2014).
51. K. Yamamura, T. Uruno, A. Shiraishi, Y. Tanaka, M. Ushijima, T. Nakahara, M. Watanabe, M. Kido-Nakahara, I. Tsuge, M. Furue, Y. Fukui, The transcription factor EPAS1 links DOCK8 deficiency to atopic skin inflammation via IL-31 induction. *Nat. Commun.* **8**, 13946 (2017).
52. M. Bunting, K. E. Bernstein, J. M. Greer, M. R. Capecchi, K. R. Thomas, Targeting genes for self-excision in the germ line. *Genes Dev.* **13**, 1524–1528 (1999).
53. T. Yamamoto, N. Takano, K. Ishikawa, M. Ohmura, Y. Nagahata, T. Matsuura, A. Kamata, K. Sakamoto, T. Nakanishi, A. Kubo, T. Hishiki, M. Suematsu, Reduced methylation of PFKFEB3 in cancer cells shunts glucose towards the pentose phosphate pathway. *Nat. Commun.* **5**, 3480 (2014).
54. Y. Sugiura, Y. Katsumata, M. Sano, K. Honda, M. Kajimura, K. Fukuda, M. Suematsu, Visualization of in vivo metabolic flows reveals accelerated utilization of glucose and lactate in penumbra of ischemic heart. *Sci. Rep.* **6**, 32361 (2016).
55. D. S. Cornett, S. L. Frappier, R. M. Caprioli, MALDI-FTICR imaging mass spectrometry of drugs and metabolites in tissue. *Anal. Chem.* **80**, 5648–5653 (2008).

Acknowledgments: We thank K. Sonoda and N. Ishimaru for valuable advice, A. Hagihara for statistical support, and A. Inayoshi and A. Aosaka for technical assistance. **Funding:** This research was supported by the Leading Advanced Projects for Medical Innovation from Japan Agency for Medical Research and Development (AMED) to Y.F. (JP18gm0010001); Grants-in-Aid for Scientific Research from the Ministry of Education, Culture, Sports, Science and Technology (to Y.F.) of Japan; and the Japan Society for the Promotion of Science (to Y.F.). Mass spectrometry infrastructure in this study was partly supported by ERATO Suematsu Gas Biology (to M.S.) from Japan Science and Technology Agency. **Author contributions:** T.S., T.U., T.T., K.Y., M.U., M.K.-N., C.M.-T., and M.W. performed functional, histological, and biochemical analyses; Y.S., Y.H., and M.S. performed mass spectrometric analyses; T.S., T.U., Y.S., M.S., and Y.F. contributed to writing the manuscript; and Y.F. conceived the project, interpreted the data, and wrote the manuscript. **Competing interests:** Kyushu University and Keio University have a pending patent application related to the work reported herein, in which Y.F., T.U., and Y.S. are listed as co-inventors. M.S. has been president of AMED since April 2015, during which time no budget for this study has been funded. All other authors declare that they have no competing interests. **Data and materials availability:** All data needed to evaluate the conclusions in the paper are present in the paper or the Supplementary Materials.

Submitted 26 July 2017
Resubmitted 14 March 2018
Accepted 9 July 2018
Published 31 July 2018
10.1126/scisignal.aao4874

Citation: T. Sakurai, T. Uruno, Y. Sugiura, T. Tatsuguchi, K. Yamamura, M. Ushijima, Y. Hattori, M. Kukimoto-Niino, C. Mishima-Tsumagari, M. Watanabe, M. Suematsu, Y. Fukui, Cholesterol sulfate is a DOCK2 inhibitor that mediates tissue-specific immune evasion in the eye. *Sci. Signal.* **11**, eaao4874 (2018).

Downloaded from http://stke.sciencemag.org/ on August 12, 2018

Science Signaling

Cholesterol sulfate is a DOCK2 inhibitor that mediates tissue-specific immune evasion in the eye

Tetsuya Sakurai, Takehito Uruno, Yuki Sugiura, Takaaki Tatsuguchi, Kazuhiko Yamamura, Miho Ushijima, Yuko Hattori, Mutsuko Kukimoto-Niino, Chiemi Mishima-Tsumagari, Mayuki Watanabe, Makoto Suematsu and Yoshinori Fukui

Sci. Signal. **11** (541), eaao4874.
DOI: 10.1126/scisignal.aao4874

Evading the immune system with a lipid

Some tissues, such as the eye, locally suppress immune cells or limit their ability to infiltrate the tissue. Sakurai *et al* . found that cholesterol sulfate (CS) inhibited the guanine nucleotide exchange factor DOCK2 and thus suppressed the migration of neutrophils and T cells in vitro. In mice, CS was produced by the gland that secretes the lipids that form the outer layer of the tear film covering the eye. Mice lacking the major sulfotransferase that produces CS from cholesterol exhibited increased infiltration of immune cells into the conjunctiva and the cornea in different in vivo models of ocular surface inflammation, which was reversed by topical application of CS. Identifying a role for CS in endogenous immunosuppression suggests that it or other bioactive lipids may play a role in other tissues that evade immune surveillance, such as tumors.

ARTICLE TOOLS http://stke.sciencemag.org/content/11/541/eaao4874

SUPPLEMENTARY MATERIALS http://stke.sciencemag.org/content/suppl/2018/07/27/11.541.eaao4874.DC1

RELATED CONTENT
http://stke.sciencemag.org/content/sigtrans/11/520/eaao1818.full
http://stke.sciencemag.org/content/sigtrans/9/419/ra29.full
http://stke.sciencemag.org/content/sigtrans/10/488/eaaf2969.full
http://science.sciencemag.org/content/sci/356/6342/1026.full
http://stm.sciencemag.org/content/scitransmed/8/328/328rv4.full
http://advances.sciencemag.org/content/advances/2/4/e1500637.full
http://advances.sciencemag.org/content/advances/4/3/eaar2766.full

REFERENCES This article cites 55 articles, 16 of which you can access for free
http://stke.sciencemag.org/content/11/541/eaao4874#BIBL

PERMISSIONS http://www.sciencemag.org/help/reprints-and-permissions

Use of this article is subject to the Terms of Service

Science Signaling (ISSN 1937-9145) is published by the American Association for the Advancement of Science, 1200 New York Avenue NW, Washington, DC 20005. 2017 © The Authors, some rights reserved; exclusive licensee American Association for the Advancement of Science. No claim to original U.S. Government Works. The title *Science Signaling* is a registered trademark of AAAS.

Downloaded from http://stke.sciencemag.org/ on August 12, 2018